Constructing a Fine Dispersion and Chemical Interface Based on an Electrostatic Self-Assembly and Aqueous Phase Compound in GO/SiO2/SBR Composites to Achieve High-Wear Resistance in Eco-Friendly Green Tires

Rui Zhang
Beijing University of Chemical Technology, Beijing, China

Jiaye Li
Beijing University of Chemical Technology, Beijing, China

Stephen Jerrams
Technological University Dublin, stephen.jerrams@tudublin.ie

See next page for additional authors

Follow this and additional works at: https://arrow.tudublin.ie/cerart

Part of the Chemical Engineering Commons, and the Polymer and Organic Materials Commons

Authors

Rui Zhang, Jiaye Li, Stephen Jerrams, Shui Hu, Shipeng Wen, and Ligun Zhang

Constructing a fine dispersion and chemical interface based on an electrostatic self-assembly and aqueous phase compound in GO/SiO₂/SBR composites to achieve high-wear resistance in eco-friendly green tires

Rui Zhang [a,c], Jiaye Li [a,c], Stephen Jerrams [b], Shui Hu [a,c], Li Liu [a,c,*], Shipeng Wen [a,c,*], Liqun Zhang [a,c]

[a] State Key Laboratory of Organic-Inorganic Composites, Beijing University of Chemical Technology, Beijing 100029, China
[b] Technological University Dublin, Dublin 00000, Ireland
[c] Beijing Engineering Research Center of Advanced Elastomers, Beijing University of Chemical Technology, Beijing 100029, China

ARTICLE INFO

ABSTRACT

The hazard to the ecosystem caused by rubber microparticles generated from tire abrasion has been a constant concern. Therefore, to protect this ecosystem, the development of a tire tread with high abrasion resistance is especially significant. Herein, γ-aminopropyltriethoxysilane (APTES) was used to modify graphene oxide (GO) and silica (SiO₂) to obtain GO and SiO₂ with positive charges (NG and NS). Furthermore, NG and NS were electrostatically self-assembled by using maleic anhydride (MAH) hydrolysis, thereby obtaining composite particles (NG-NS) with "bridged structures". Also, the NG-NS/styrene butadiene rubber (SBR) compounds possessing fine dispersion of NG-NS were prepared by the aqueous compounding method. During the crosslinking process, the vinyl groups in NG-NS reacted with the vinyl groups of the SBR molecule chains, thus forming strong chemical interfacial interactions between the NG-NS and rubber macromolecules. Compared with an SiO₂/SBR composite, the 300 % modulus, tensile strength, abrasion resistance of the NG-NS/SBR composite were improved by 125 %, 122 %, 83.3 %, respectively. Compared with a GO/SiO₂/SBR composite, heat build-up in the NG-NS/SBR was decreased by 8.2 °C.

1. Introduction

At present, the hazard of microplastics to ecosystem has attracted more and more attention in many countries [1]. Rubber particles generated from tire abrasion are the major contributor to the total microplastic release [2–4]. According to reports, 0.96 ± 0.35 kg/capita of rubber particles were discharged into the natural environment in 2008 [5]. 74 % of these rubber particles were deposited into the soil, 22 % of them flowed into surface water and 4 % of them floated in the air [5]. Predominantly in research into this phenomenon, toxic metals and organic compounds were detected from filtrate of tire abrasion particles [6], including zinc, polycyclic aromatic hydrocarbons (PAHs), polychlorinated biphenyls (PCBs), benzothiazoles, chlorinated paraffins [7–13]. PAHs are considered by the European Chemicals Agency (ECHA) as persistent organic pollutants, and give rise to properties such as carcinogenic, bioaccumulative toxicity [14]. Tire abrasion plastics input to the environment has been quantified in several studies

[3,6,7,15]. Without development of new tire materials, it is evident that the environmental pollution caused by tire abrasion particles will continue to accumulate in the ecosystem. Consequently, the preparation of tires with high abrasion resistance is of great significance for protecting the ecosystem.

The abrasion resistance of rubber composites is determined by several factors which primarily comprise two aspects: (1) Hysteresis and heat build-up of rubber composites [16], as during the driving of a vehicle, tire temperatures rise sharply due to the internal friction of rubber composites during repeated deformation. This results in a large number of unsaturated double bonds and active allyl hydrogens being degraded under the attack of thermo-oxidation [17–19]. (2) Dispersion of nanofillers in rubber matrices and interfacial interaction between nanofillers and rubber molecules [20] where the rubber molecule chains are fixed on the surface of the nanofillers to form adsorption layers, which is beneficial in enhancing the strength and abrasion resistance of these rubber composites [21–23]. The strength of the adsorption layer
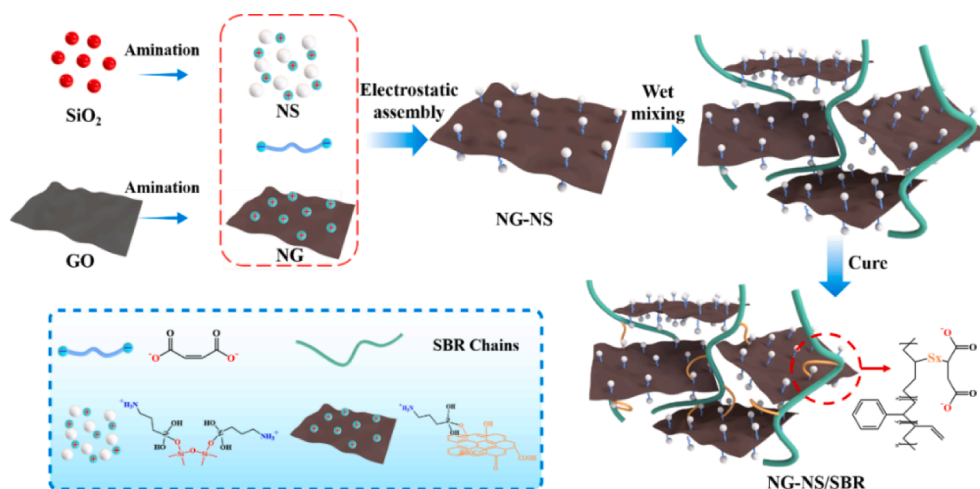

Fig. 1. Schematic of the preparation process of NG-NS/SBR composites.
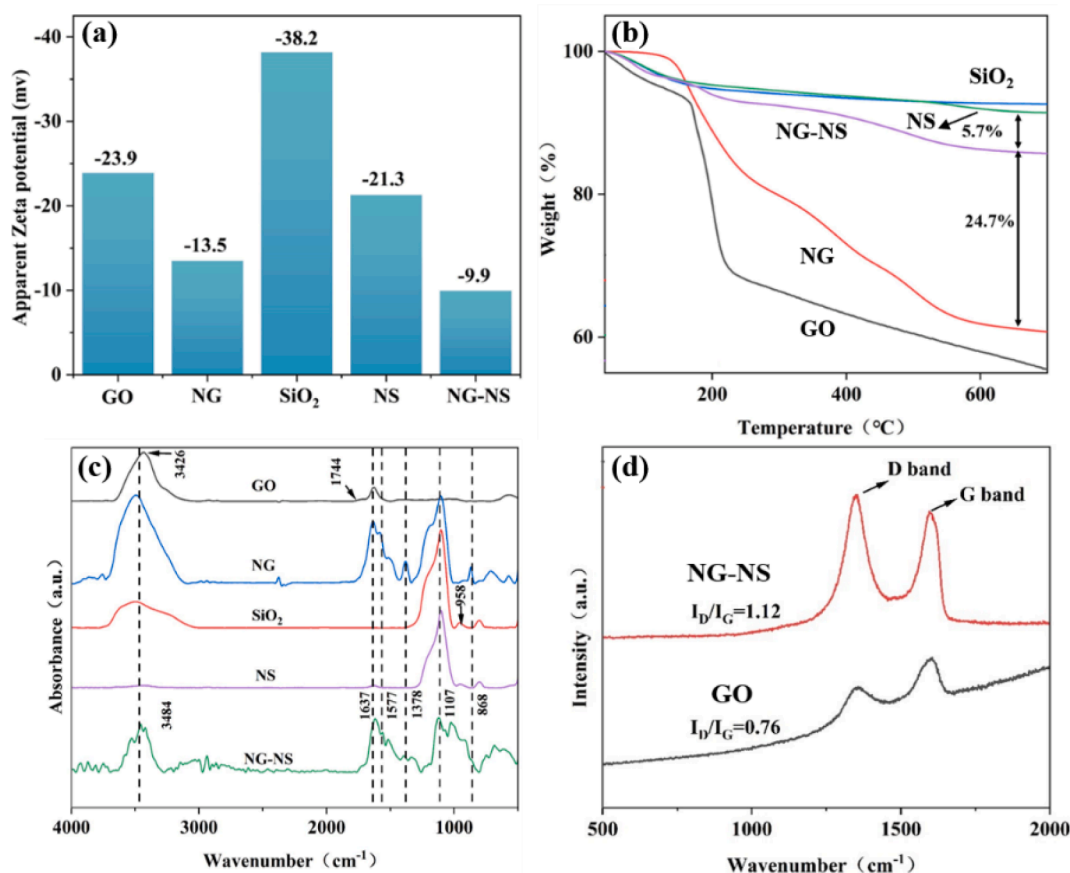

Fig. 2. (a) Zeta potential, (b) TGA curves, (c) FTIR spectra of GO, SiO_2, NG, NS, NG-NS and (d) Raman spectra of GO and NG-NS.

mainly depends on the interfacial interaction between nanofillers and rubber molecular chains. Consequently, it is crucial to improve these properties to heighten the abrasion resistance of tires.

Until now, nano-silica was generally used to strengthen static mechanical properties and abrasion resistance of rubber composites [24–26], so unsurprisingly, the surface modification of silica has gained the attention of numerous researchers. Tian et al. [27]. used hexamethyl disilazane (HMDS) to modify nano-silica by employing the liquid phase in-situ method. HMDS-capped nano-silica has improved dispersibility in rubber matrices as well as enhancing compatibility and interfacial interaction with the rubber molecular chains. This research exhibited an

improvement of abrasion resistance in the rubber composites of 18.4 %. Zhu et al. [28] prepared silica grafted sodium xanthate (SSX) by catalyzed hydroxyl groups in silica. SSX was homogeneously dispersed in a natural rubber (NR) matrix compared with the traditional aggregated silica. The abrasion resistance performance of the rubber composites was improved by more than 50 %, when the SSX content was 0.9 phr.

Two-dimensional layered graphene oxide (GO), has a large specific surface area [29]. Compared with spherical SiO_2, the movement of rubber molecular chains is more easily constrained by GO sheets. Meanwhile, GO provides excellent mechanical and wear properties for rubber composites. Jin et al. [30] synthesized zinc-free coupling agents
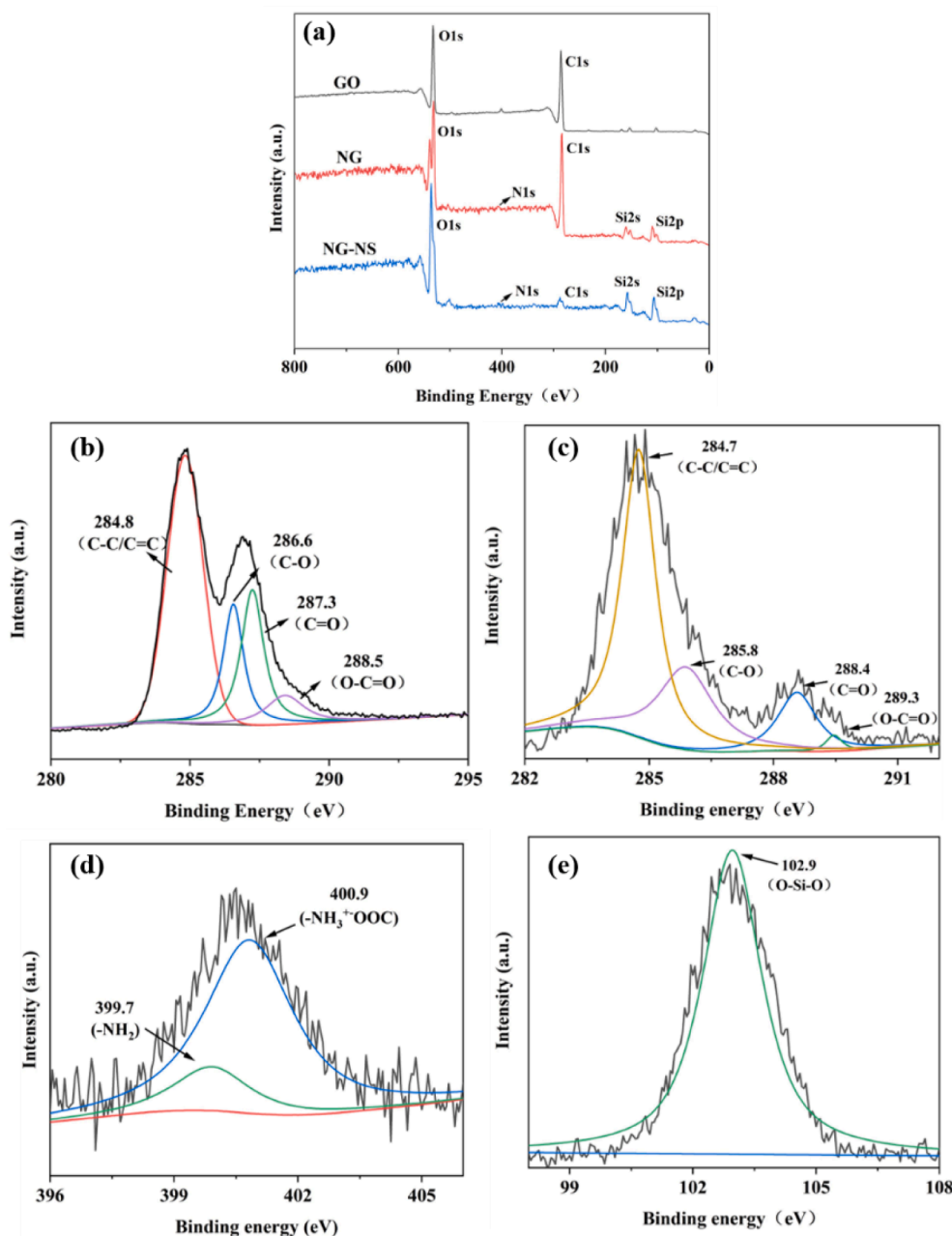
Fig. 3. (a) XPS survey scans of GO, NG and NG-NS (b) the C1s XPS spectrum of GO, (c) the C1s XPS spectrum of Ng-NS, (d) the N1s XPS spectrum of NG-NS, and (e) the Si2p XPS spectrum of NG-NS.

(ZFCs) and ZFCs-functionalized graphene (GZFCs), and fabricated GZFCs-embedded SBR. In high-speed endurance testing, the pneumatic tires made with the GZFCs/SBR composite showed high abrasion resistance and low rolling resistance, due to high dispersity and strong interfacial interaction of CZFCs in the silica/rubber matrix. Yang et al. [31] designed a covalent interface in a graphene/elastomer by introducing tea polyphenols (TP) modified and reduced GO (TP-rGO). The DIN abrasion of the TP-rGO/SBR composite was improved by up to 40 % due to the excellent dispersion and strong covalent interface provided by the TP-rGO. The research projects discussed here all focused on improving the filler-dispersion and interfacial interaction of rubber composites merely filled by silica or graphene. As such, silica and graphene are both required to enhance the abrasion properties of rubber composites. Therefore, creating a fine filler dispersion and chemical interface in rubber composites filled with silica and graphene simultaneously is crucial to improving abrasion properties.

In our previous research [32], the SBR masterbatch containing highly dispersed GO was prepared by the emulsion compounding method. Thereafter, a further compound with SiO_2 was fabricated by the mechanical blending method to provide a $GO/SiO_2/SBR$ composite. Compared with the SiO_2/SBR composite, the abrasion resistance and rolling resistance of the $GO/SiO_2/SBR$ composite were both improved which can be attributed to the fine dispersion and strong interfacial interaction of GO, as opposed to silica in the rubber matrix. Therefore, it is still a difficult challenge to simultaneously achieve a fine dispersion and strong interfacial interaction caused by GO and SiO_2 to result in the high abrasion resistance and reduction in heat build-up that is required.

In this research, the novel composite particles (NG-NS) with "bridged structures", composed of maleic anhydride (MAH), surface modified graphene oxide (NG) and silica (NS) with positive charges, were fabricated. NG-NS was further introduced into SBR matrix to obtain NG-NS/SBR composites. The NG and NS with negative charges were well
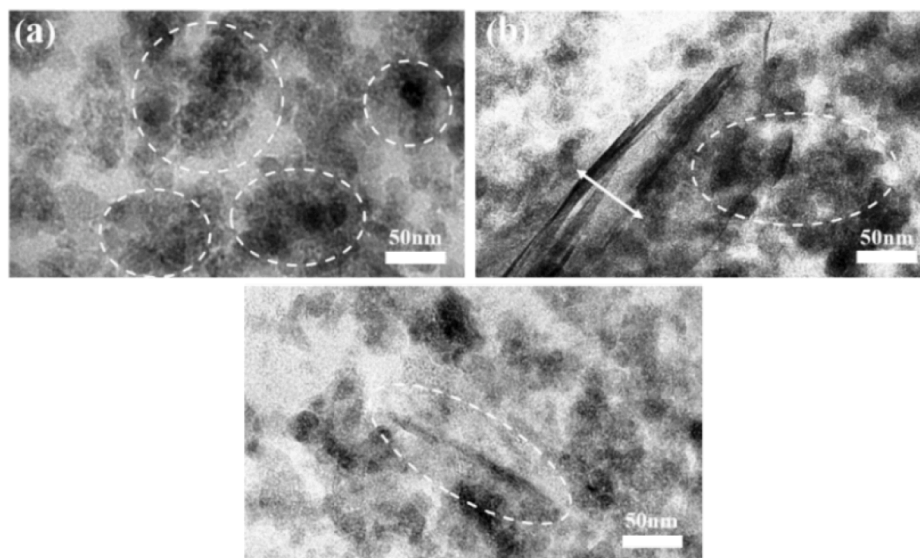
Fig. 4. TEM images of (a) SiO$_2$/SBR, (b) GO/SiO$_2$/SBR and (c) NG-NS/SBR composites.
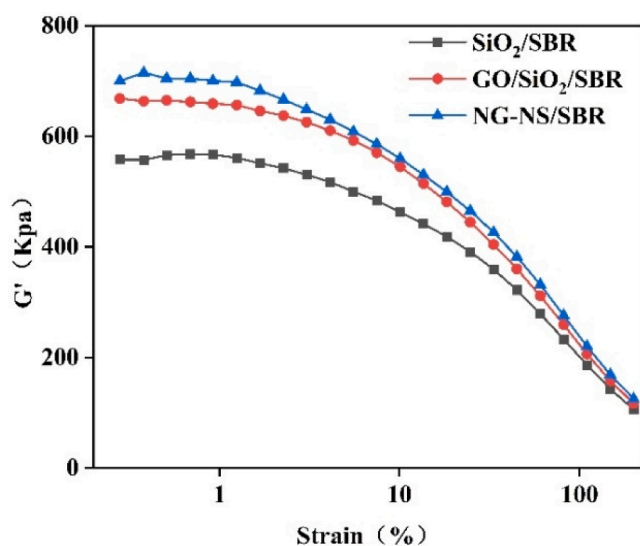
Fig. 5. Energy storage modulus-strain curves of SiO$_2$/SBR, GO/SiO$_2$/SBR and NG-NS/SBR compounds.

dispersed in the SBR matrix due to the repulsive force between the two fillers. Importantly, the NG-NS particles with C=C bonds in MAH were further grafted into the rubber molecule chain to strengthen the interfacial interaction between the NG-NS and SBR molecules. The new structure of NG-NS composite endows the NG-NS/SBR composites possessed excellent mechanical properties, high wear properties and low heat build-up.

2. Experimental Section

2.1. Materials

GO was synthesized by a modified Hummers method. γ-aminopropyltriethoxysilane (APTES) was provided by Beijing Mairuida Technology Co., ltd (China). Styrene-butadiene rubber latex (SBR, 1502) was purchased from Shandong Xianyuan Technology Co., ltd (China). The solid content of SBR was 21 wt%. Zinc oxide (ZnO), Stearic acid (SA), N-1,3-dimethylbutyl-N`-phenyl-p-phenylenediamine (6ppd),

polymerized 2,2,4-trisilica (VN3), *N*-Cyclohexyl-2-benzothiazolesulfenamide (CZ) and sulfur were all commercially available and used without any treatment.

2.2. Samples preparation

2.2.1. Preparation of NG and NS

A 2 mg/ml GO suspension was prepared by sonication for 30 min. The APTES deionized water/ethanol (1/9, v/v) was added to the GO suspension (m$_{GO}$/m$_{APTES}$ = 1/2.5). Then the mixture was stirred for 1 h, resulting in hydrolysis of the ethoxy groups on the APTES to generate highly reactive silanol groups. After reaction at 68 °C for 6 h, the mixture was washed several times by using a centrifugal machine to remove the unreacted APTES. After Soxhlet extraction, the modified GO was again mixed with the deionized water to form a 2 mg/ml suspension which was labeled NG.

Silica suspension with smaller particle sizes were prepared by placing the silica dispersions in a colloid mill at 1200 r/min for 20 min. Subsequently, silica was also modified by APTES. A 100 g/L suspension was prepared by a similar procedure with GO suspension, and labled NS.

2.2.2. Preparation of NG-NS

The homogeneous suspension of NG and NS was mixed and sonicated for 1 h. After MAH was completely hydrolyzed, the MAH hydrolysate solution (mol$_{MAH}$/mol$_{APTES}$ = 0.5:1) was added to the mixture of NG and NS. After reaction at 90 °C for 6 h, the mixture was washed several times by using a centrifugal machine to remove the unreacted MAH hydrolysate. The mixture of NG and NS was again mixed with deionized water to obtain a homogeneous suspension, which was labled NG-NS.

2.2.3. Preparation of rubber composites

A controlled amount of SiO$_2$ (45 phr), GO/SiO$_2$ (48 phr) and NG-NS (48 phr) were mixed with the SBR latex by agitation for 20 min, and then the mixture was flocculated by CaCl$_2$ solution (1.5 wt%). After the flocculated mixture was washed several times using deionized water, the SiO$_2$/SBR, GO/SBR and NG-NS/SBR compounds were obtained. Afterwards, the SiO$_2$/SBR, GO/SBR and NG-NS/SBR compounds were compounded with 3 parts per hundred rubber (phr) ZnO, 2 phr SA, 2 phr 6ppd, 2 phr poly(1,2-dihydro-2,2,4-trimethyl-quinoline) (antioxidant RD), 2 phr *N*-cyclohexylbenzothiazole-2-sulphenamide (Accelerator CZ) and 1.8 phr sulfur on a two-roll mill to obtain the SiO$_2$/SBR, GO/SBR and NG-NS/SBR compounds. Finally, the SiO$_2$/SBR, GO/SBR and NG-NS/SBR composites were obtained after curing at 151 °C under a
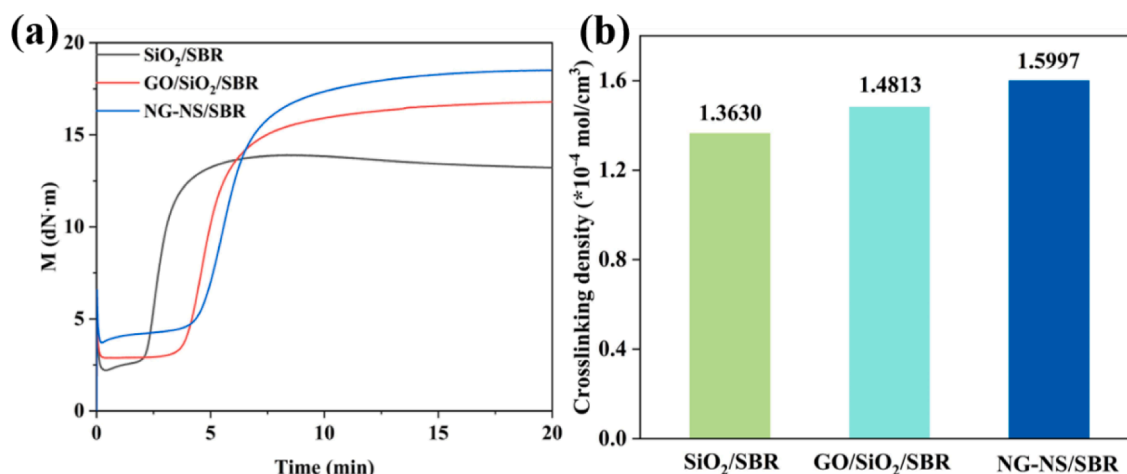
Fig. 6. (a) Torque dependency (M) on time curves and (b) cross-link densities of SiO$_2$/SBR, GO/SiO$_2$/SBR and NG-NS/SBR composites.

Table 1
Vulcanization Properties of SiO$_2$/SBR, GO/SiO$_2$/SBR and NG-NS/SBR composites.

Sample	T$_{90}$ (min)	MH (dN·m)	ML (dN·m)	MH-ML
SiO$_2$/SBR	4.28	13.36	1.96	11.40
GO/SiO$_2$/SBR	8.29	16.83	2.69	14.14
NG-NS/SBR	9.11	18.52	3.43	15.09

pressure of 15 Mpa.

2.3. Characterization

The morphologies of GO, SiO$_2$, NG-NS and the dispersion of different fillers in SBR composites were observed using G220 S-TWIN transmission electron microscopy (TEM, FEI Co., USA). Surface regularity of GO and NG-NS was characterized by an Invia Raman (Renishaw Co., England). The laser wavelength was 514 nm and the laser intensity was 10 %. Spectra were recorded within wavenumbers ranging from 500 to 2000 cm^{-1}. Elemental analysis of GO and NG-NS was performed by using an ESCALAB 250 X-ray photoelectron spectroscope (XPS, Thereto Electron Co., USA). C, O, N and Si, were scanned using an Al Kα X-ray source (1486.6 eV). The chemical structures of GO, SiO$_2$, NG-NS were recorded by a Tensor 27 Fourier transform infrared (FTIR) spectrometer (Bruker Optik Gmbh Co., Germany). Spectra were recorded within wavenumbers ranging from 400 to 4000 cm^{-1}. Zeta potential of all samples was characterized by a Laser particle analyzer (Malvern Instruments Co., England). The weight loss of all samples was identified using a TGA-1 thermal gravimetric analyzer (Mettler-Toledo Co., Switzer-land). The TGA test was performed at a heating rate of 10 °C /min under a nitrogen atmosphere. The filler network structure of all rubber compounds was characterized by RPA 2000 (Alpha Technologies Co. USA). For rubber compounds, the strain range was 0.1–200 %, the test frequency was set to 1 Hz, and the temperature of the test was set at 60 °C. The dynamic mechanical properties of rubber composites were investigated using a VA3000 dynamic mechanical thermal analyzer (DMTA, METRAVIB Corporation, France). The tests were performed in tensile mode at 10 Hz. The temperature ranged from −80 to 80 °C at a heating rate of 3 °C/min. The rectangular samples used in this testing had dimensions of approximately 10 mm × 6 mm × 1 mm. Three samples for each composite were prepared for DMA testing. The static mechanical performances of rubber composites were characterized by a CTM4104 electrical tensile tester (Shenzhen SANS Test Machine Co., China), in accordance with ISO 37:2005 standard. Abrasion performance of rubber composites was tested using a GT-7012-D DIN abrasion

machine (Mingzhu Machinery Co., ltd., China) in accordance with ISO 4649: 2002. Heat build-up of rubber composites was characterized by a Goodrich flexometer (BF Goodrich Co., USA). The heat build-up samples were 25 mm in height and 18 mm in diameter. The ambient temperature of the heat build-up samples was 55 °C. The compression frequency experienced by the heat build-up samples was 55 Hz and the stroke was 4.45 mm. The temperature rise at the specimen base was recorded.

3. Results and discussion

### 3.1. Design and preparation of NG-NS/SBR composites

The design and preparation of the NG-NS/SBR composites are schematically illustrated in Fig. 1. The GO and silica possessing positive charges were obtained in the aqueous phase by the modification of γ-aminopropyltriethoxysilane (APTES), resulting in a repulsive force between the two fillers and avoiding filler aggregation. Thereafter, MAH hydrolysis, having negative charge, was introduced to bridge silica and GO by electrostatic self-assembly, forming NG-NS composite particles in the aqueous phase. Further, NG-NS aqueous dispersion was compounded with SBR latex particles to obtain a mixture solution with fine NG-NS dispersion. Subsequently, the NG-NS/SBR composites with fine dispersion were prepared by co-coagulation. During the vulcanization process, the NG-NS particles with C=C bonds in MAH were further grafted into the rubber molecule chain to strengthen the interfacial interaction between the NG-NS and SBR molecules (see the "Experimental Section" for a detailed process).

3.2. Characterizations of NG-NS

To verify the success of electrostatic assembly between NG, NS and MAH, the zeta potential tests in Fig. 2a was used to examine the surface charges of GO, SiO$_2$, NG, NS and NG-NS. All samples are negatively charged. Compared with that of GO and SiO$_2$, the increased zeta potential values of NG and NS indicated the silanol groups of APTES hydrolysate reacted with negatively charged groups on the surface of GO and SiO$_2$. The hydrolysate product of MAH was maleic acid, which ionizes in the aqueous solution to form –COO$^-$ groups. Therefore, the potential of the aqueous solution of MAH was negative. However, the zeta potential value of NG-NS was much higher than that of NG and NS, suggesting that the strong electrostatic bonding resulted in a reduction in negative charges and formation of NG-NS composite particles with a sandwich-like structure.

Fig. 2b shows the TGA curves of GO, SiO$_2$, NG, NS and NG-NS. SiO$_2$ exhibits extremely high thermal stability and its slight weight loss is mainly attributed to the evaporation of bound water [33]. The 8.0 %
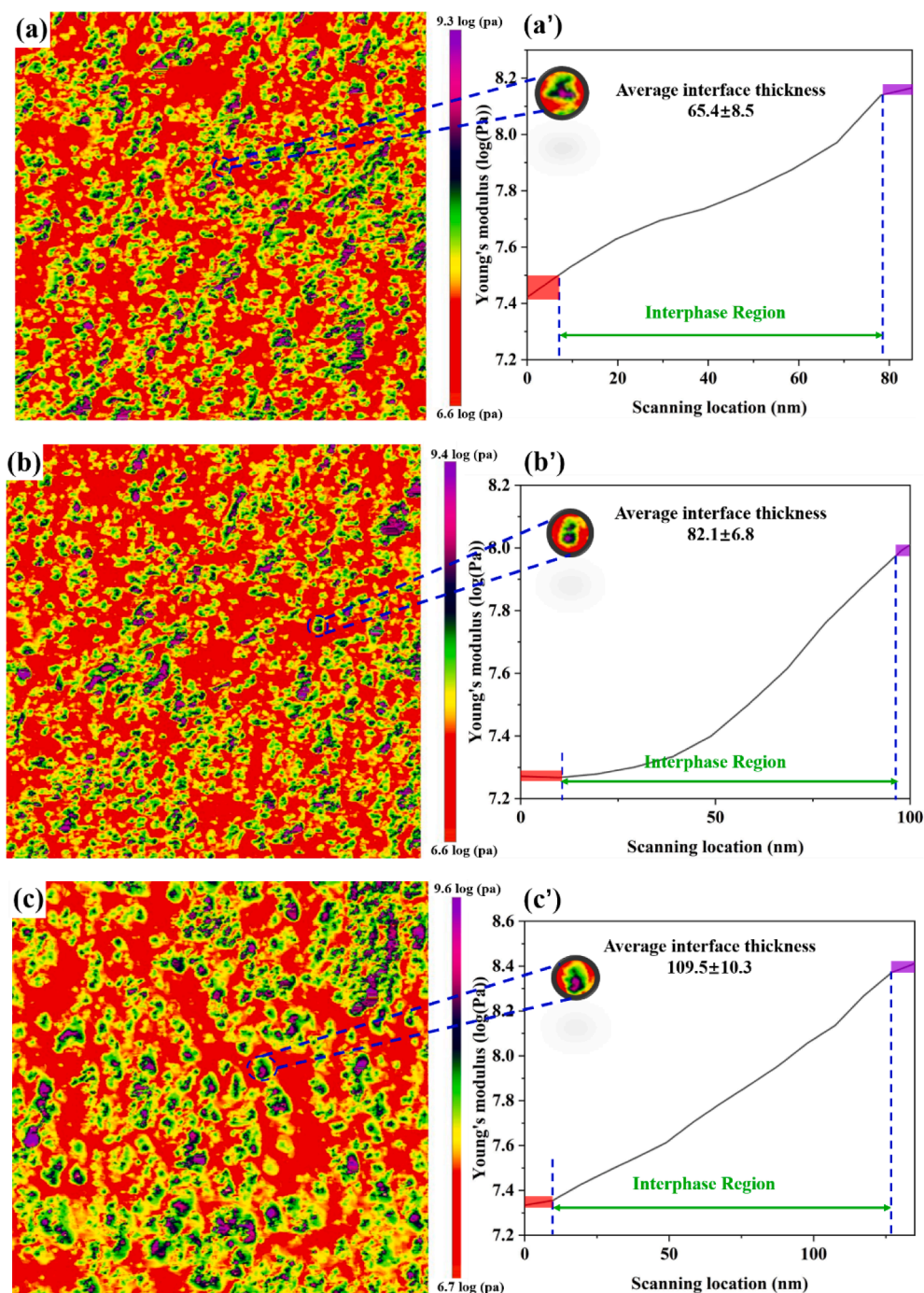
Fig. 7. Young's modulus maps of (a) SiO$_2$/SBR, (b) GO/SiO$_2$/SBR and (c) NG-NS/SBR composites and their corresponding modulus profiles (a'), (b') and (c') across the interphase, respectively.

weight loss of NS was largely attributed to the evaporation of bound water and the decomposition of silane molecules. The thermal decomposition of GO was divided into three stages: [34] The first was the water evaporation stage at 40–160 °C. The bound water adsorbed by the oxygen-containing functional groups on the surface of GO was evaporated in this stage. The second was the decomposition of oxygen-containing groups at 160–240 °C. The third was the rearrangement of the unstable carbocyclic structure and the disintegration of the carbon skeleton in GO at 240–700 °C. Finally, the GO weight loss was 47.6 %. In the case of NG, the main weight loss was due to the decomposition of oxygen-containing groups and silane molecules at 140–550 °C. The weight loss (13.7 %) of NG-NS is lower than that (38.4 %) of NG, which

is mainly due to the presence of SiO$_2$ in NG-NS.

Fig. 2c shows that the FTIR spectra of GO, SiO$_2$ and NG-NS. In the spectrum for GO, the peaks at 3426, 1744 and 1622 cm^{-1} are attributed to the O—H, C=O and C=C stretching vibrations, respectively [35]. In the spectrum for SiO$_2$, the peaks at 1107 and 868 cm^{-1} are both ascribed to the stretching and bending vibration of Si–O [36,37]. In addition, the peak at 958 cm^{-1} is attributed to the Si-OH stretching vibration. By comparison with GO and SiO$_2$, the new peaks for NS, NG and NG-NS at 1378–1637 cm^{-1} are attributed to the N—H, C—H and C—N stretching or bending vibrations, indicating their successful functionalization [36,38,39]. In addition, the peak of –NH$_2$ variable angle vibration of NG-NS was shifted from 1577 to 1565 cm^{-1}, suggesting a faint
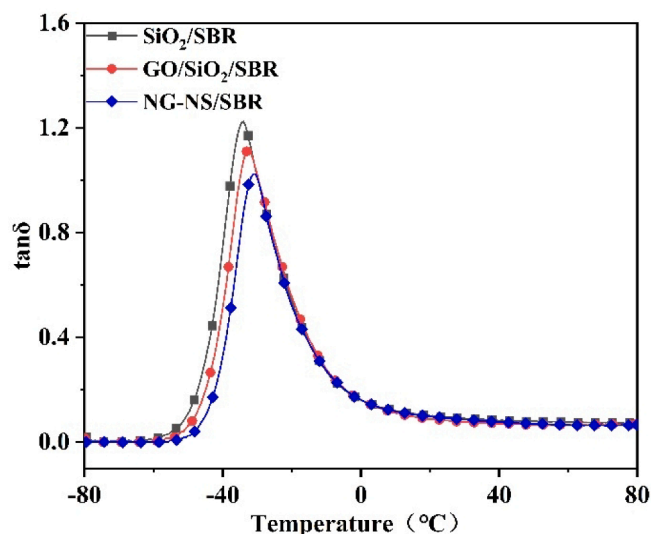
Fig. 8. The loss factors versus temperature curves of SiO$_2$/SBR, GO/SiO$_2$/SBR, and NG-NS/SBR composites.

Table 2
The loss factors of SiO$_2$/SBR, GO/SiO$_2$/SBR, and NG-NS/SBR composites at 60 °C and 0 °C.

Temperature	SiO$_2$/SBR	GO/SiO$_2$/SBR	NG-NS/SBR
0 °C	0.156	0.160	0.161
60 °C	0.076	0.066	0.064

Table 3
The constrained region (*C*) of SiO$_2$/SBR, GO/SBR, and NG-NS/SBR composites.

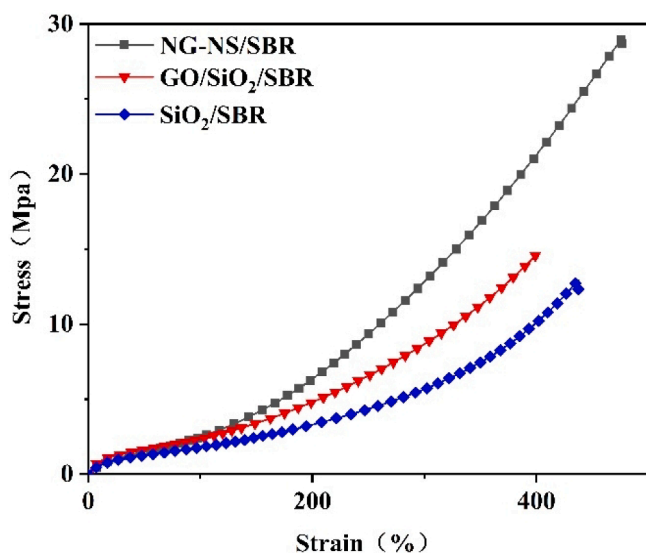| Samples	SiO$_2$/SBR	GO/SiO$_2$/SBR	NG-NS/SBR
C values	0.031	0.050	0.069

Fig. 9. Stress–strain curves of SiO$_2$/SBR, GO/SiO$_2$/SBR, and NG-NS/SBR composites.

electrostatic interaction between –NH$_2$ and –COOH[36,40]. It was noted that the peak at 3464 cm^{-1} was wider and higher due to the overlapping of the O—H and NH$_2$ stretching vibration.

Fig. 2d shows that the Raman spectra of GO and NG-NS. The spectra of GO and NG-NS showed peaks located at 1344 and 1593 cm^{-1} for the D band and G band, respectively [41]. The ratio of I$_D$/I$_G$ increases from 0.76 for GO to 1.12 for NG-NS, illustrating that the structural integrity of GO sheets was destroyed after electrostatic self-assembly with SiO$_2$.

XPS spectra in Fig. 3 were employed to characterize the surface chemical composition of GO, NG and NG-NS. Fig. 3a shows that the full spectra of GO, NG and NG-NS, indicating that the characteristic peaks of silicon and nitrogen elements appear in NG and NG-NS. Fig. 3b and c show the XPS C1s spectra of GO and NG-NS. Three fitted peaks of NG-NS at 285.8, 288.4 and 289.3 eV correspond to C—O, C=O and O-C=O, respectively [42]. For NG-NS, the intensity of peaks of C—O, C=O and O-C=O decreased sharply compared with NG, due to the GO surface being covered by SiO$_2$ particles. Fig. 3d shows that the peak of –NH$_3^+$OOC appeared in the N1s XPS spectra, indicating that the electrostatic attraction between carboxyl groups on the MAH hydrolysate and amino groups on the NG and NS [38]. Si2p spectra in Fig. 3e shows the peak of O-Si-O appeared in NG-NS particles, suggesting that NS was attached to the surface of NG [43].

3.3. Dispersion of NG-NS in SBR matrix

To explore the dispersion of fillers in rubber composites, TEM was performed on the surface of the samples. As shown in Fig. 4a and b, SiO$_2$ particles and GO sheets appeared to undergo severe stacking and agglomeration in the rubber composites. As for NG-NS/SBR in Fig. 4c, the agglomeration of SiO$_2$ particles and the stacking of GO sheets were significantly reduced, suggesting that electrostatic repulsion between fillers promoted the dispersion of fillers in the SBR matrix.

3.4. Filler network in the NG-NS/ SBR composite

Fig. 5 shows the filler networks in SiO$_2$/SBR, GO/SiO$_2$/SBR and NG-NS/SBR compounds. The SiO$_2$/SBR compound had the lowest energy storage modulus among the three compounds. This is because there was a large amount of agglomeration of SiO$_2$ particles in the SBR matrix, resulting in the reduction of the specific surface area of SiO$_2$, and the poor interfacial interaction between SiO$_2$ particles and rubber molecular chains. The energy storage modulus of GO/SiO$_2$/SBR compounds was higher than that of SiO$_2$/SBR composites, indicating that the constraint effect of GO sheets on rubber molecular chains was much greater than that of the SiO$_2$ particles. NG-NS/SBR has the highest storage modulus, attributed to GO sheets and SiO$_2$ particles both having a fine dispersion in the SBR matrix. The constrictions on the movement of SBR molecules by GO and SiO$_2$ were stronger than those in the other compounds [44]. Therefore, the dispersibility of the fillers and the shape of the filler play a crucial role in the construction of the filler network.

Curing tests of different SBR composites were performed at 150 °C on different SBR composites and the resulting curves are presented in Fig. 6a and Table 1. The torque of the NG-NS/SBR composite changed maximally within 20 min and then increased slightly compared to GO/SiO$_2$/SBR, indicating the crosslinking reaction between NG-NS and SBR occurred and a weak three-dimensional crosslinking network formed. Fig. 6b shows that crosslinking density of NG-NS/SBR composite is higher than that of SiO$_2$/SBR and GO/SiO$_2$/SBR composites, revealing that a grafting reaction may occur between the vinyl groups in maleic anhydride (MAH) and C=C bonds in the rubber molecules.

3.5. Interfacial interaction between NG-NS and SBR molecules

The PF-QNM technique was used to measure the gradient change of Young's modulus of the SiO$_2$/SBR, GO/SiO$_2$/SBR, and NG-NS/SBR composites. The thickness of interphases between nanofiller and SBR molecule chains was evaluated quantitatively. Fig. 7 shows the average interphase thicknesses of NG-NS/SBR composite (109.5 ± 10.3 nm) were much higher than those of SiO$_2$/SBR (65.4 ± 8.5 nm), GO/SiO$_2$/

Table 4
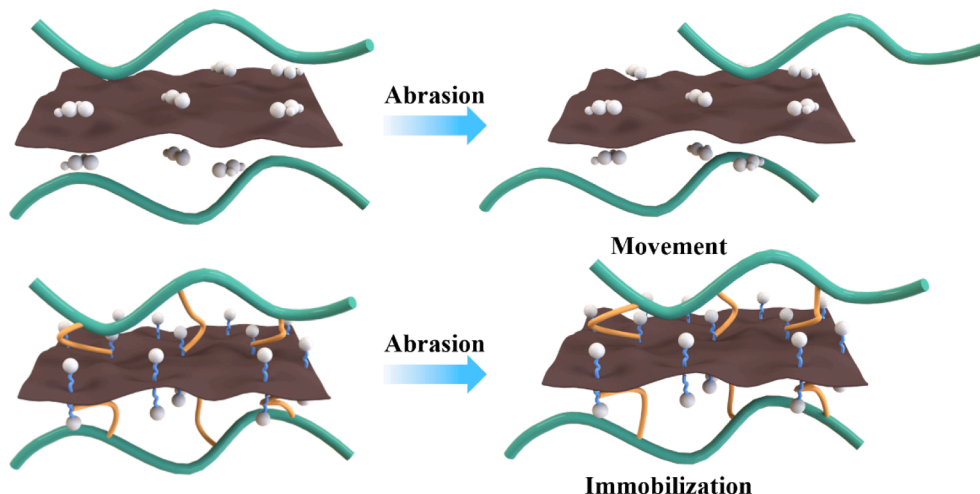Mechanical properties of SiO$_2$/SBR, GO/SiO$_2$/SBR, and NG-NS/SBR composites.

Samples	Shore A hardness	100 % Modulus (Mpa)	300 % Modulus (Mpa)	Tensile strength (Mpa)	Elongation at break (%)	Tear strength (kN/m)
SiO$_2$/SBR	66 ± 1	1.8 ± 0.1	5.7 ± 0.4	12.9 ± 0.3	437 ± 15	31.6 ± 1.1
GO/SiO$_2$/SBR	75 ± 1	2.4 ± 0.1	8.7 ± 0.3	14.6 ± 0.4	399 ± 18	45.4 ± 1.3
NG-NS/SBR	67 ± 1	2.5 ± 0.1	12.8 ± 0.1	28.7 ± 0.6	476 ± 19	55.7 ± 1.2

Table 5
Comparison of mechanical properties with different SBR composites filled with silica and GO (or rGO).

Samples	300 % Modulus (Mpa)	Tensile strength (Mpa)	Elongation at break (%)	Tear strength (kN/m)
NG-NS/SBR	12.8	28.7	476	55.7
TP-rGO/SBR [31]	11.8	21.5	530	35.1
SBR/SG [38]	2.7	17.6	850	32.0
1 %rGO/SiO$_2$ [29]	12.5	24.8	442	47.5
CBSi5 [48]	–	12.6	752	35.7
SBR/DeVulcNR/ SiO$_2$(30)/GO (3) [49]	–	12.7	828	32.6
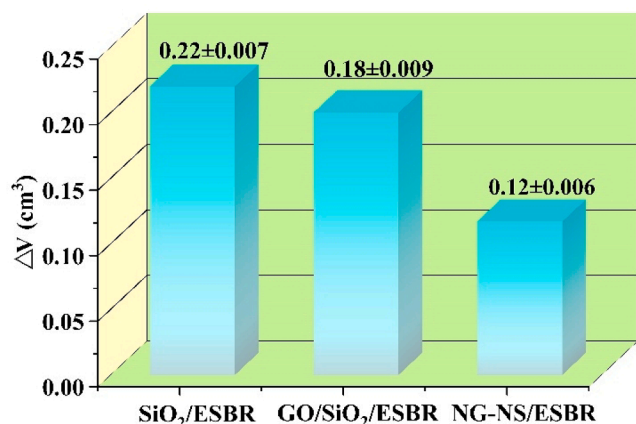
Fig. 10. DIN abrasions of SiO$_2$/SBR, GO/SiO$_2$/SBR and NG-NS/SBR composites.

SBR (82.1 ± 6.8 nm), respectively. The high interphase modulus and thickness are beneficial for transferring the external forces and distributing the stress, subsequently enhancing the abrasion resistance [45].

DMA was used to investigate the interfacial interaction between the filler and SBR molecules. Fig. 8 shows that the peak value of the loss factor of the NG-NS/SBR composite was the lowest among the three samples, and the glass transition temperature of the NG-NS/SBR composite moved to a higher temperature compared with that of SiO$_2$/SBR composite. This is because the vinyl group of MAH hydrolysates in NG-NS was grafted with the vinyl groups of SBR in the presence of sulfur during the curing process at high temperature. The graft reaction promoted the formation of strong interfacial interaction between the NG-NS and SBR matrix and limited the movement of SBR molecules. Table 2 shows the NG-NS/SBR composite had the lowest loss factor at 60 °C and the highest loss factor at 0 °C, indicating that the rolling resistance and wet skid resistance of the NG-NS/SBR composite were superior among the three samples [45].

As reported, SBR composites exhibited linear viscoelasticity at high nanofiller content [46]. The linear viscoelasticity behavior was represented by the relationship between the volume fraction of the constrained region (C) and the loss factor (tanδ). The dynamic viscoelastic equation is as follows:

$$C = 1 - (1 - C_0)W/W_0 \tag{1}$$

where C_0 and W_0 represent the energy fraction loss and volume fraction of the constrained region for pure SBR, respectively. Here, C_0 is taken to be 0 and W is the energy loss fraction of the composites, calculated using the following equation: [47].

$$W = \pi \tan\delta / (\pi \tan\delta + 1) \tag{2}$$

The C values of the composites containing different kinds of fillers were calculated and compared in Table 3. The C values of the NG-NS/SBR (0.069) composite was much higher than that of SiO$_2$/SBR (0.031) and GO/SiO$_2$/SBR (0.050), suggesting the NG-NS filler effectively limited rubber molecules and promoted the interfacial interaction with the rubber matrix.
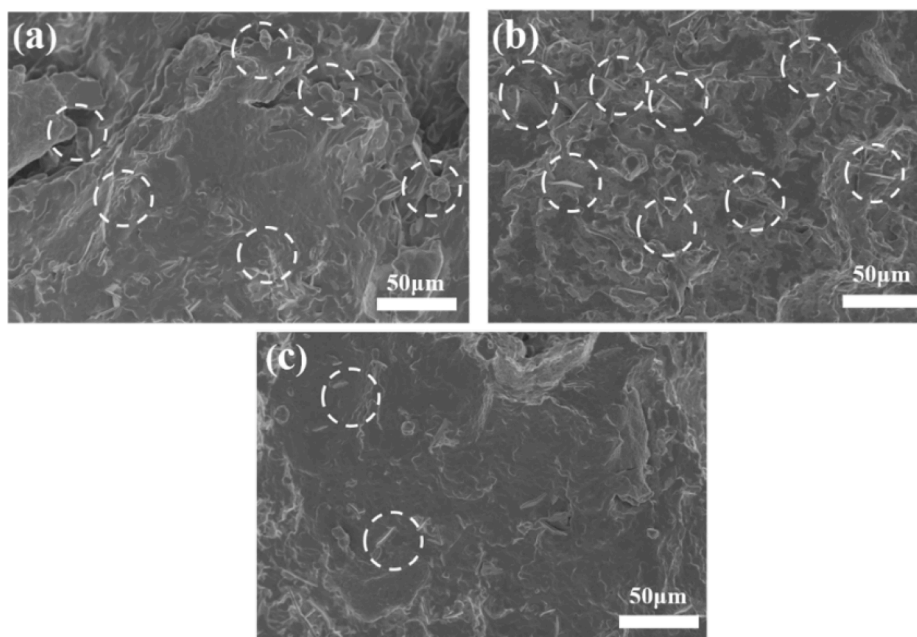

Fig. 11. The mechanism diagram of abrasion resistance of GO/SiO$_2$/SBR and NG-NS/SBR composites.

Fig. 12. SEM images of the DIN abrasion surfaces of (a) SiO$_2$/SBR, (b) GO/SiO$_2$/SBR and (c) NG-NS/SBR composites.
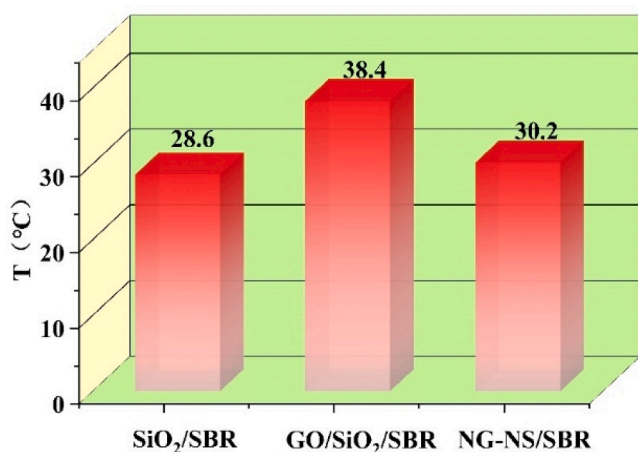

Fig. 13. Heat build-up SiO$_2$/SBR, GO/SiO$_2$/SBR, NG-NS/SBR composites.

3.6. Static mechanical properties of NG-NS/SBR composite

Fig. 9 and Table 4 show the static mechanical properties of different SBR composites. The 300 % tensile modulus, tensile strength of NG-NS/SBR composite were increased by 125 %, 122 %, respectively, compared with those of SiO$_2$/SBR composite. This improvement was due to the fine dispersion of NG-NS filler and the chemical interface constructed by the graft reaction between NG-NS and SBR molecules. Thus, stronger and more solid interaction sites between filler and rubber molecules were formed, which was beneficial to the force transmission, and improved the mechanical properties of the NG-NS/SBR composite. In addition, it was found the 300 % modulus, tensile strength, elongation at break and tear strength of NG-NS/SBR were higher than those of other similar systems filled with silica and GO (or rGO) in Table 5, attributing to the fine dispersion of NG-NS and the chemical interface in NG-NS/SBR composites.

3.7. Abrasion resistance and abrasion surface topography of NG-NS/SBR composites

Fig. 10 shows the DIN abrasion resistances of different SBR composites. The abrasion resistance of the NG-NS/SBR composite showed an improvement 45.5 %, compared with that of the SiO$_2$/SBR composite. Fig. 11 shows the improvement mechanism of abrasion resistance for SBR composites. During the abrasion process of the rubber composites, rubber molecules slipped and were migrated and broken when subjected to the external forces [50–52]. Therefore, the improvement in the abrasion resistance of NG-NS/SBR was attributed to two factors: (1) The contact area between nanofiller and rubber molecules was increased due to the high dispersion of the GO and SiO$_2$ in the SBR matrix, resulting in the movement of most of the rubber molecules being constrained by nanofillers. (2) The increased modulus of adsorption layer on the nanofiller surface led to the rubber molecule chains being further immobilized. Therefore, SBR molecules in the NG-NS/SBR composite were not easily broken, finally leading to the high abrasion resistances.

3.8. Abrasion surface topography of NG-NS/SBR composites

SEM was employed to characterize the surface topography of SiO$_2$/SBR, GO/SiO$_2$/SBR and NG-NS/SBR composites after DIN abrasion was carried out. In Fig. 12a and b, the surfaces of SiO$_2$/SBR and GO/SiO$_2$/SBR are seen to be relatively rough. More abrasion strips were observed on the surface of SiO$_2$/SBR and GO/SiO$_2$/SBR composites. This was because the mutual contact area between nanofillers and rubber molecules was reduced in the SiO$_2$/SBR and GO/SiO$_2$/SBR composites, due to poor filler dispersion in the SBR matrix. The physical adsorption of the filler to the rubber molecular chains was not beneficial in respect of sharing the external shear forces.

In contrast, Fig. 12c shows the much smoother surface of the NG-NS/SBR composite when compared with that of SiO$_2$/SBR and GO/SiO$_2$/SBR composites. This was assumed to be because the external forces were evenly shared due to the formation of more physical and chemical crosslinking points by the fine dispersion of NG-NS, and the chemical interfacial interaction between NG-NS and rubber molecular chains. The uniform network reduced the possibility of slippage and breakage of SBR molecules, resulting in the improvement of abrasion resistance.

3.9. Heat build-up in NG-NS/SBR composites

Three variants of nanoscale friction are primarily responsible for the heat build-up of rubber composites. These are friction between polymer chains and nanoparticles, between nanoparticles and nanoparticle and between polymer chains and polymer chains [53]. Fig. 13 shows that the heat build-up temperature of the GO/SiO$_2$/SBR composite increased by 9.8 °C compared with that of the SiO$_2$/SBR composite, suggesting that there is significant mutual friction between GO sheets and SiO$_2$ particles. However, the heat build-up temperature of the NG-NS/SBR composite decreased by 8.2 °C compared with that of the GO/SiO$_2$/SBR composite, indicating that high dispersion and a strong interfacial interaction contributed to the reduction in friction between all components. Especially, the reduction in the friction between fillers was attributed to two factors: (1) MAH hydrolysate acted as a "lubricant" between GO sheets and SiO$_2$ particles to reduce the friction between their surfaces. (2) The grafting reaction occurred between the vinyl groups in NG-NS and C=C bonds in the rubber molecules, resulting in a strong interfacial interaction between the filler and the rubber molecules. The collisions possibilities between fillers decreased, thereby reducing the friction between fillers.

4. Conclusions

In this study, SBR compound with a fine dispersion of GO and SiO$_2$ was prepared by aqueous compounding and electrostatic self-assembly. During the vulcanization process that followed, MAH hydrolysates in NG-NS formed irreversible cross-linked bonds with the C=C bonds in the rubber molecules, promoting an interfacial interaction between NG-NS and SBR molecules. Compared with SiO$_2$/SBR composites, the 300 % modulus, tensile strength and abrasion resistance of NG-NS/SBR composites were improved by 125 %, 122 %, 83.3 %, respectively. Compared with GO/SiO$_2$/SBR composites, heat build-up in the NG-NS/SBR declined by 8.2 °C. This novel aqueous compound system and interface design provide a new and novel opportunity for preparing high-performance rubber composites with high abrasion resistance.

Declaration of Competing Interest

The authors declare that they have no known competing financial interests or personal relationships that could have appeared to influence the work reported in this paper.

Data availability

Data will be made available on request.

Acknowledgments

References

[1] D.K. Barnes, F. Galgani, R.C. Thompson, M. Barlaz, Accumulation and fragmentation of plastic debris in global environments, Philos. Trans. R. Soc. Lond. B Biol. Sci. 364 (1526) (2009) 1985–1998.

[2] N.B. Hartmann, T. Huffer, R.C. Thompson, M. Hassellov, A. Verschoor, A. E. Daugaard, S. Rist, T. Karlsson, N. Brennholt, M. Cole, M.P. Herrling, M.C. Hess, N.P. Ivleva, A.L. Lusher, M. Wagner, Are We Speaking the Same Language? Recommendations for a Definition and Categorization Framework for Plastic Debris, Environ. Sci. Technol. 53 (3) (2019) 1039–1047.

[3] P.J. Kole, A.J. Lohr, F. Van Belleghem, A.M.J. Ragas, Wear and Tear of Tyres: A Stealthy Source of Microplastics in the Environment, Int. J. Environ. Res. Public Health 14 (10) (2017) 1265.

[4] F.D. Boucher, J,, Primary Microplastics in the Oceans, A Global Evaluation of Sources (2017).

[5] R. Sieber, D. Kawecki, B. Nowack, Dynamic probabilistic material flow analysis of rubber release from tires into the environment, Environ. Pollut. 258 (2020), 113573.

[6] A. Wik, G. Dave, Occurrence and effects of tire wear particles in the environment–a critical review and an initial risk assessment, Environ. Pollut. 157 (1) (2009) 1–11.

[7] S. Wagner, T. Huffer, P. Klockner, M. Wehrhahn, T. Hofmann, T. Reemtsma, Tire wear particles in the aquatic environment - A review on generation, analysis, occurrence, fate and effects, Water Res. 139 (2018) 83–100.

[8] B. Bocca, G. Forte, F. Petrucci, S. Costantini, P. Izzo, Metals contained and leached from rubber granulates used in synthetic turf areas, Sci. Total Environ. 407 (7) (2009) 2183–2190.

[9] M. Llompart, L. Sanchez-Prado, J. Pablo Lamas, C. Garcia-Jares, E. Roca, T. Dagnac, Hazardous organic chemicals in rubber recycled tire playgrounds and pavers, Chemosphere 90 (2) (2013) 423–431.

[10] L.M. Daniele Coppola, Release of Polycyclic Aromatic Hydrocarbons and Heavy Metals from Rubber Crumb in Synthetic Turf Fields: Preliminary Hazard Assessment for Athletes, Journal of Environmental & Analytical, Toxicology 05 (02) (2014) 1000265.

[11] S.H. Brandsma, M. Brits, Q.R. Groenewoud, M.J.M. van Velzen, P.E.G. Leonards, J. de Boer, Chlorinated Paraffins in Car Tires Recycled to Rubber Granulates and Playground Tiles, Environ. Sci. Technol. 53 (13) (2019) 7595–7603.

[12] E. Skoczynska, P.E.G. Leonards, M. Llompart, J. de Boer, Analysis of recycled rubber: Development of an analytical method and determination of polycyclic aromatic hydrocarbons and heterocyclic aromatic compounds in rubber matrices, Chemosphere 276 (2021), 130076.

[13] D. Armada, M. Llompart, M. Celeiro, P. Garcia-Castro, N. Ratola, T. Dagnac, J. de Boer, Global evaluation of the chemical hazard of recycled tire crumb rubber employed on worldwide synthetic turf football pitches, Sci. Total Environ. 812 (2022), 152542.

[14] D. Armada, M. Celeiro, T. Dagnac, M. Llompart, Green methodology based on active air sampling followed by solid phase microextraction and gas chromatography-tandem mass spectrometry analysis to determine hazardous substances in different environments related to tire rubber, J. Chromatogr. A 1668 (2022), 462911.

[15] F. Sommer, V. Dietze, A. Baum, J. Sauer, S. Gilge, C. Maschowski, R. Gieré, Tire Abrasion as a Major Source of Microplastics in the Environment, Aerosol Air Qual. Res. 18 (8) (2018) 2014–2028.

[16] X. Chen, Y. Kong, M. Wang, X. Huang, Y. Huang, Y. Lv, G. Li, Wear and aging behavior of vulcanized natural rubber nanocomposites under high-speed and high-load sliding wear conditions, Wear 498–499 (2022), 204341.

[17] J.I.C.T. Colclough, G.M.C., Higgins, Oxidative aging of natural rubber vulcanizates. Part III, J. Appl. Polym. Sci. 12 (2) (1968) 295–307.

[18] J.I. Cunneen, Oxidative aging of natural rubber, Rubber Chem. Technol. 41 (1) (1968) 182–208.

[19] E.B.M.E.J. Blackman, Relationships between the structures of natural rubber vulcanizates and their thermal and oxidative aging, Rubber Chem. Technol. 43 (3) (1970) 651–663.

[20] L. Chu, M. Kan, S. Jerrams, R. Zhang, Z. Xu, L. Liu, S. Wen, L. Zhang, Constructing Chemical Interface Layers by Using Ionic Liquid in Graphene Oxide/Rubber Composites to Achieve High-Wear Resistance in Environmental-Friendly Green Tires, ACS Appl. Mater. Interfaces 14 (4) (2022) 5995–6004.

[21] V.A. Froltsov, M. Kluppel, G. Raos, Molecular dynamics simulation of rupture in glassy polymer bridges within filler aggregates, Phys Rev E Stat Nonlin Soft Matter Phys 86 (4 Pt 1) (2012), 041801.

[22] S. Yang, J. Choi, M. Cho, Elastic stiffness and filler size effect of covalently grafted nanosilica polyimide composites: molecular dynamics study, ACS Appl. Mater. Interfaces 4 (9) (2012) 4792–4799.

[23] K.W. Stöckelhuber, A.S. Svistkov, A.G. Pelevin, G. Heinrich, Impact of Filler Surface Modification on Large Scale Mechanics of Styrene Butadiene/Silica Rubber Composites, Macromolecules 44 (11) (2011) 4366–4381.

[24] Y. Zou, J. He, Z. Tang, L. Zhu, F. Liu, Structural and mechanical properties of styrene–butadiene rubber/silica composites with an interface modified in-situ using a novel hindered phenol antioxidant and its samarium complex, Compos. Sci. Technol. 188 (2020).

[25] Y. Shui, L. Huang, C. Wei, G. Sun, J. Chen, A. Lu, L. Sun, D. Liu, How the silica determines properties of filled silicone rubber by the formation of filler networking and bound rubber, Compos. Sci. Technol. 215 (2021), 109024.

[26] B. Yoon, J.Y. Kim, U. Hong, M.K. Oh, M. Kim, S.B. Han, J.-D. Nam, J. Suhr, Dynamic viscoelasticity of silica-filled styrene-butadiene rubber/polybutadiene rubber (SBR/BR) elastomer composites, Compos. B Eng. 187 (2020), 107865.

[27] Q. Tian, C. Zhang, Y. Tang, Y. Liu, L. Niu, T. Ding, X. Li, Z. Zhang, Preparation of hexamethyl disilazane-surface functionalized nano-silica by controlling surface chemistry and its "agglomeration-collapse" behavior in solution polymerized styrene butadiene rubber/butadiene rubber composites, Compos. Sci. Technol. 201 (2021), 108482.

[28] K. Zhu, Y. Liu, H. Wang, X. Guo, S. Liao, Z. Wang, L. Fang, Xanthate-modified silica as a novel multifunctional additive for properties improvement of natural rubber, Compos. Sci. Technol. 203 (2021), 108567.

[29] H. Zhu, Z. Wang, X. Huang, F. Wang, L. Kong, B. Guo, T. Ding, Enhanced comprehensive performance of SSBR/BR with self-assembly reduced graphene oxide/silica nanocomposites, Compos. B Eng. 175 (23) (2019) 207–219.

[30] J.G. Seo, C.K. Lee, D. Lee, S.H. Song, High-performance tires based on graphene coated with Zn-free coupling agents, J. Ind. Eng. Chem. 66 (2018) 78–85.

[31] Z. Yang, J. Liu, R. Liao, G. Yang, X. Wu, Z. Tang, B. Guo, L. Zhang, Y. Ma, Q. Nie, F. Wang, Rational design of covalent interfaces for graphene/elastomer nanocomposites, Compos. Sci. Technol. 132 (2016) 68–75.

[32] Y. Mao, S. Wen, Y. Chen, F. Zhang, P. Panine, T.W. Chan, L. Zhang, Y. Liang, L. Liu, High performance graphene oxide based rubber composites, Sci. Rep. 3 (2013) 2508.

[33] R. Azimi, H. Roghani-Mamaqani, M. Gholipour-Mahmoudalilou, Grafting poly (amidoamine) dendrimer-modified silica nanoparticles to graphene oxide for preparation of a composite and curing agent for epoxy resin, Polymer 126 (2017) 152–161.

[34] X. Liu, D. Sun, L. Wang, B. Guo, Sodium Humate Functionalized Graphene and Its Unique Reinforcement Effects for Rubber, Ind. Eng. Chem. Res. 52 (41) (2013) 14592–14600.

[35] H. Wang, H. Zhang, J. Zhang, Y. Zhao, Improving tribological performance of fluoroether rubber composites by ionic liquid modified graphene, Compos. Sci. Technol. 170 (2019) 109–115.

[36] L. Cao, T.K. Sinha, L. Tao, H. Li, C. Zong, J.K. Kim, Synergistic reinforcement of silanized silica-graphene oxide hybrid in natural rubber for tire-tread fabrication: A latex based facile approach, Compos. B Eng. 161 (2019) 667–676.

[37] M. Wang, L. Ma, L. Shi, P. Feng, X. Wang, Y. Zhu, G. Wu, G. Song, Chemical grafting of nano-SiO2 onto graphene oxide via thiol-ene click chemistry and its effect on the interfacial and mechanical properties of GO/epoxy composites, Compos. Sci. Technol. 182 (26) (2019) 197–209.

[38] Y. Lin, S. Liu, J. Peng, L. Liu, The filler–rubber interface and reinforcement in styrene butadiene rubber composites with graphene/silica hybrids: A quantitative correlation with the constrained region, Compos. A Appl. Sci. Manuf. 86 (22) (2016) 19–30.

[39] Q.G. Yan Xu, H. Liang, Kangsheng Zheng, Effects of functional graphene oxide on the properties of phenyl silicone rubber composites, Polym. Test. 168 (175) (2016) 54.

[40] S. Bulou, E. Lecoq, F. Loyer, G. Frache, T. Fouquet, M. Gueye, T. Belmonte, P. Choquet, Study of a pulsed post-discharge plasma deposition process of APTES: synthesis of highly organic pp-APTES thin films with NH2 functionalized polysilsesquioxane evidences, Plasma Processes Polym. 16 (4) (2019) 1800177.

[41] Z. Xu, S. Jerrams, L. Zheng, L. Zhang, L. Liu, S. Wen, Green Fabrication of High-Performance, Lignosulfonate-Functionalized, and Reduced-Graphene Oxide Styrene-Butadiene Rubber Composites, Ind. Eng. Chem. Res. 60 (49) (2021) 17989–17998.

[42] S. Stankovich, R.D. Piner, X. Chen, N. Wu, S.T. Nguyen, R.S. Ruoff, Stable aqueous dispersions of graphitic nanoplatelets via the reduction of exfoliated graphite oxide in the presence of poly(sodium 4-styrenesulfonate), J. Mater. Chem. 16 (2) (2006) 155–158.

[43] M. Du, B. Guo, Y. Lei, M. Liu, D. Jia, Carboxylated butadiene–styrene rubber/ halloysite nanotube nanocomposites: Interfacial interaction and performance, Polymer 49 (22) (2008) 4871–4876.

[44] C. Zhang, Z. Tang, B. Guo, L. Zhang, Significantly improved rubber-silica interface via subtly controlling surface chemistry of silica, Compos. Sci. Technol. 156 (2018) 70–77.

[45] X. Zhai, Y. Chen, D. Han, J. Zheng, X. Wu, Z. Wang, X. Li, X. Ye, L. Zhang, New designed coupling agents for silica used in green tires with low VOCs and low rolling resistance, Appl. Surf. Sci. 558 (2021), 149819.

[46] J. Diani, P. Gilormini, Y. Merckel, F. Vion-Loisel, Micromechanical modeling of the linear viscoelasticity of carbon-black filled styrene butadiene rubbers: The role of the filler–rubber interphase, Mech. Mater. 59 (2013) 65–72.

[47] X. Zhang, L.S. Loo, Study of Glass Transition and Reinforcement Mechanism in Polymer/Layered Silicate Nanocomposites, Macromolecules 42 (14) (2009) 5196–5207.

[48] D.Z. Pirityi, T. Bárány, K. Pölöskei, Hybrid reinforcement of styrene-butadiene rubber nanocomposites with carbon black, silica, and graphene, J. Appl. Polym. Sci. 139 (32) (2022).

[49] D. Mondal, S. Ghorai, D. Rana, D. De, D. Chattopadhyay, The rubber–filler interaction and reinforcement in styrene butadiene rubber/devulcanize natural rubber composites with silica–graphene oxide, Polym. Compos. 40 (S2) (2018) E1559–E1572.

[50] J. Chen, J. Liu, Y. Yao, S. Chen, Effect of microstructural damage on the mechanical properties of silica nanoparticle-reinforced silicone rubber composites, Eng. Fract. Mech. 235 (2020), 107195.

[51] P.B.E. Padenko, B. Wetzel, J. Karger-Kocsis, Mechanical and abrasion wear properties of hydrogenated nitrile butadiene rubber of identical hardness filled with carbon black and silica, J. Reinf. Plast. Compos. 35 (1) (2015) 81–91.

[52] S.T. Paveena Tangudom, N. Sombatsompop, Cure and mechanical properties and abrasive wear behavior of natural rubber, styrene–butadiene rubber and their blends reinforced with silica hybrid fillers, Mater. Des. 53 (3) (2014) 856–864.

[53] X. Qin, H. Xu, G. Zhang, J. Wang, Z. Wang, Y. Zhao, Z. Wang, T. Tan, M. R. Bockstaller, L. Zhang, K. Matyjaszewski, Enhancing the Performance of Rubber with Nano ZnO as Activators, ACS Appl. Mater. Interfaces 12 (42) (2020) 48007–48015.